Encinas-Sánchez, V.; Batuecas, E.; Macías-García, A.; Mayo, C.; Díaz, R.; Pérez, F.J. (2018). Corrosion resistance of protective coatings against molten nitrate salts for thermal energy storage and their environmental impact in CSP technology, *Solar Energy*, v. 176, pp.: 688-697.

DOI: https://doi.org/10.1016/j.solener.2018.10.083

Corrosion resistance of protective coatings against molten nitrate salts for thermal energy storage and their environmental impact in CSP technology

V. Encinas-Sánchez[a,*], E. Batuecas[a], A. Macías-García[b], C. Mayo[a], R. Díaz[c], F.J. Pérez[a]

[a] Surface Engineering and Nanostructured Materials Research Group, Complutense University of Madrid, Complutense Avenue s/n, 28040 Madrid, Spain
[b] Deparment of Mechanical, Energetic and Materials Engineering. School of Industrial Engineering, University of Extremadura, Avda. de Elvas, s/n, 06006 Badajoz, Spain
[c] Open University of Madrid, UDIMA, Faculty of Technical Sciences and Engineering, Road A-6, 15, exit 36, 28400 Collado Villalba, Madrid, Spain

Sol-gel ZrO_2–3%molY_2O_3 coating deposited by means of a dip-coating application on P91 steel was statically tested at 500 °C in contact with Solar Salt (60% wt.% $NaNO_3$/40 wt.% of KNO_3) for 1000 h. This work assessed the behaviour of the coated P91 steel both from a technical and environmental point of view. Both studies were compared to those obtained with AISI 304 steel, which is currently used in commercial CSP plants. In terms of corrosion evaluation, the behaviour of the coated P91 was directly comparable to that of the uncoated AISI 304, SEM micrographs revealing the better behaviour of coated samples and the maintenance of a compact coating layer, with a thickness ranging between 1 and 1.4 μm. Furthermore, environmental analyses revealed the environmental benefits obtained by using lower Cr-Ni content steel coated with ZrO_2–Y_2O_3 compared to AISI 304 alloy, since this coating had a negligible environmental impact (its influence is below 0.03%). Thus, the proposed scenario seems to be workable in CSP high-temperature applications both from technical and environmental points of view. The linked technical-environmental quantification provided in this paper highlights the importance of considering the whole assessment when conducting material selection for CSP applications

1. Introduction

Nowadays there is an increasing demand for renewable energy (Fuqiang et al., 2017), solar energy being a vast, sustainable, and clean source of energy (Jin et al., 2017). Among the solar technologies, Concentrated Solar Power (CSP) is considered a promising technology (Vignarooban et al., 2015; Giglioa et al., 2017) and the number of studies in the field is increasing rapidly (de Miguel et al., 2016; García-Martín et al., 2017; Grosu et al., 2018). The main target is the improvement of the dispatchability of this technology (Grosu et al., 2018). Thermal energy storage (TES) appears as a realistic solution for enabling CSP to be a dispatchable source of renewable energy (Liu et al., 2016). Molten nitrate salts are currently considered ideal candidates for both heat transfer and storage applications because of their properties. Nowadays, the best industrial compound is considered to be an alkali metal nitrate mixture composed of 60 wt.% $NaNO_3$/40 wt.% KNO_3 (Solar Salt®) (Dorcheh et al., 2016).

Although CSP has reached technological maturity, the high costs present a strategic challenge. To reduce them, highly efficient, integrated and cheaper CSP materials are urgently needed (Pizzolato et al., 2015). Nowadays, stainless steels are widely used in commercial CSP plants due to their well-known physicochemical and mechanical properties (Dorcheh et al., 2016). Several studies have been performed to understand their corrosion behaviour under molten salt environments (Dorcheh et al., 2016; Bradshaw and Goods, 2001; Goods and Bradshaw, 2004). Dorcheh et al. (2016) found the formation of thin oxide scales (composed of a two layer structure) in SS316 and SS347H, this following similar kinetics. Bradshaw and Goods (2001) and Goods and Bradshaw (2004) calculated annualized rates of metal loss between 6 and 15 μm/year for SS304, SS316 and SS316L specimens at 565 °C depending on the particular salt mixture. Among stainless steels, it is important to highlight AISI 304 stainless steel (Zaversky et al., 2013), which was used at the Solar Two project for the hot tank (Pacheco et al., 2002). However, these steels are known for their high cost in comparison with other steels (Ruiz-Cabañas et al., 2017). Ferritic-martensitic steels would be a suitable alternative from the economical point of view. Nevertheless, from a technological point of view, these steels do not offer a sufficient long-term corrosion resistance in contact with molten nitrate salts (Dorcheh et al., 2016). Dorcheh et al. (2016) studied two low chromium alloys, P91 and X20CrMoV, and found rapid corrosion rates in the mass gain curves, the weight gain being 21.1 and 18.1 m cm^{-2} after 2500 h at 600 °C, respectively. Thus, the

development of protective coatings for low alloyed steels, such as P91, could be an economical alternative for increasing the lifetime of pipes and tanks in CSP plants against molten salt corrosion. This solution would allow CSP plants to reduce the Levelized cost of electricity (LCOE), which is one of the major objectives currently set (González-Roubaud et al., 2017).

Regarding the coating process, sol-gel coatings present numerous advantages (Wang and Bierwagen, 2009; Choudhury and Agrawal, 2011), including the low processing temperature and the possibility of depositing on complex shapes. The basis of this process is to coat a substrate with a precursor solution containing the coating material in the required proportion, allowing solvent evaporation and/or chemical reactions to transform it to a gel layer (John-Berlin et al., 2014). One of the most commonly used sol-gel protective coatings consists of oxides, yttrium-stabilized zirconia (YSZ) being a great option because of its properties (Díaz-Parralejo et al., 2010). Zirconia shows excellent thermal shock resistance, mechanical and chemical properties (Kamalan-Kirubaharan et al., 2018). The use of Y_2O_3 as stabilizer im- proves the thermal stability and anti-aging performance (Encinas- Sánchez et al., 2017), this leading to the excellent high-temperature phase stability of YSZ (Kamalan-Kirubaharan et al., 2018). With respect to the deposition of sol-gel solutions, there are several methods (Johnson et al., 2005; Amri et al., 2012). Dip-coating in particular is an easy deposition technique that allows the preparation of uniform coatings through simple control of the withdrawal rate at low cost (Mimura and Kato, 2013). Dip-coating technique consists in immersing the sample to be coated in the sol-gel solution, which allows coating surfaces in different dimensions (Encinas-Sánchez et al., 2017).

On the other hand, environmental issues are urgent and critical today. Therefore, in the improvement of CSP plants, it is important to take into account not only technical and economic criteria but also the ecological and environmental impact (Batuecas et al., 2017). In this respect, the steel industry is an important cause of overall anthropogenic greenhouse gas emissions (Eloneva et al., 2010). Although the steel industry has the technical potential to reduce its energy consumption by approximately 20% by applying the best available technology (He and Wang, 2017), many old steel production plants and not all new plants apply this technology. Therefore, the most effective strategy for reducing the global environmental impacts of steel manufacturing will be based on a suitable choice of materials. This means minimising the use of steels with higher environmental impacts. The reduction in the use of such steels will lead to an effective decrease in environmental damage. In this scenario, Life Cycle Assessment (LCA) appears to be a suitable tool for analysing environmental effects in a comprehensive way.

Historically, the industry has focused on technical development issues. The introduction of the environmental pillar as another physico-chemical variable is now necessary for achieving full sustainable development. Thus, this study was focused on the evaluation of protective coatings on ferritic-martensitic steels, while integrating a variable that is increasingly important and in keeping with the spirit of the solar power plants: overall sustainability. To this end, ZrO_2–Y_2O_3 sol-gel coatings were deposited on P91 steel and tested in contact with Solar Salt at 500 °C for up to 1000 h. This system was also studied from an environmental point of view using LCA. Both technical and environmental results were compared to the results obtained with AISI 304 steel, which is currently used in commercial CSP plants.

2. Methodology

2.1. Materials

2.1.1. Preparation of the salt mixture and substrates

The chemicals used in this experiment were sodium nitrate ($NaNO_3$) (99%, BASF) and potassium nitrate (KNO_3) (98%, Haifa). The main impurities in both nitrates are gathered in Table 1. These nitrates were mixed according to the commercial composition, 60 wt.% $NaNO_3$/ 40 wt.% KNO_3, known as Solar Salt®, which is the most widely-used salt mixture in solar power plants (Zhao and Wu, 2011).

Table 1
Main impurities in the chemicals used.

Chemicals	Cl^-, %	SO_4^{2-}, %	CO_3^{2-}, %
$NaNO_3$	0.02	0.005	0.02
KNO_3	0.015	< 0.0005	< 0.02

Regarding the substrates, two types, including AISI 304 stainless steel and P91 ferritic-martensitic steel, were used in this study as materials for CSP applications. Table 2 shows the chemical composition in wt.% of AISI 304 and P91 steels. As gathered, P91 is characterized by a low percentage of Cr (~9%) compared to AISI 304 (~18%). The test pieces were fabricated to a size of 20 × 10 × 2 mm^3, superficially rectified and ground (with sandpapers to P180). The size of the test pieces was selected on the basis of previous works (de Miguel et al., 2016; García-Martín et al., 2017; Encinas-Sánchez et al., 2018), these dimensions being suited to the corrosion test crucibles used. The treatment on each surface was carried out for 5 min at a force of 30 N, this being followed by ultrasonic cleaning with alcohol and de-ionized water. The low-grade sandpapers were selected to provide uniform surface finish to all samples and to avoid surface irregularities from manufactures.

2.1.2. Sol-gel preparation and deposition

The 3 mol% yttria–doped zirconia sol-gel solution was prepared in accordance with a previously reported procedure (Encinas-Sánchez et al., 2017; Encinas-Sánchez et al., 2016).

The deposition of the yttria–doped zirconia coatings was only performed on the P91 substrates. This deposition was carried out in air by using the dip-coating technique. The deposition parameters were selected according to a previously reported study (Encinas-Sánchez et al., 2015). Thus, coatings were obtained at a withdrawal rate of 25 mm min^{-1} and sintered at 500 °C. The sintering process was carried out in a Hobersal® oven for 2 h by applying heating/cooling rates of 3 °C min^{-1}. This slow heating/cooling ramp inhibits crack formation by relaxing the stress arising from crystallization and thermal expansion without causing fissures (Hamden et al., 2014). Prior to the heat-treatment, the coated samples were dried in the oven at 100 °C for 60 min, applying the same heating/cooling rate. This prior drying phase minimizes the content of organic residues in the coating, thus leading to a reduction in stress in the coating (Croll, 1979).

Once prepared, coated samples were characterized by Scanning Electron Microscopy–Energy Dispersive X-Ray Spectroscopy (SEM-EDX) using a JEOL® JSM-820 scanning electron microscope.

2.2. Corrosion study

2.2.1. Corrosion tests

The corrosion tests were performed in an electrical chamber furnace (Carbolite®) at 500 °C with the specimens placed in alumina crucibles and fully immersed in the salt mixture to a melt depth of about 3.5 cm. The working temperature was selected on the basis of previous analyses of the salt carried out by thermogravimetric analysis (TGA). TGA was performed using a SDT-Q600 from TA Instruments. To perform this analysis, 10 mg of salt mixture were placed in crucibles made of platinum and opened to atmosphere. The test was conducted at a heating rate of 10 °C min^{-1} and a flowing air atmosphere of 100 ml m^{-1} was used. Prior to the analyses, the instrument was calibrated with indium.

During the corrosion test, the samples were analysed via a gravimetric method at 0, 24, 72, 168, 250, 500, 750, and 1000 h. Three samples of each system were removed at each selected time and were slowly cooled and rinsed with warm distilled water to remove the

Table 2
Chemical composition (in wt.%) of AISI 304 and P91 steels.

Substrate	C	Si	Mn	P	S	Al	Cr	Mo	Ni	V	N	Nb	Cu	Co
P91	0.12	0.21	0.49	0.014	0.002	0.01	8.7	0.85	0,02	0.18	0.053	0.06	–	–
AISI 304	0.04	0.36	1.4	0.04	0.012	–	18.29	0.18	8.19		0.078	–	0.19	0.1

remaining salt. They were then dried and weighed and an average was taken from five weight values. The formula (Eq. (1)) used to calculate the mass gain over time:

$$\frac{\Delta m}{S_0} = \frac{m_f - m_i}{S_0} \quad (1)$$

where m_i is the initial mass of the specimen, m_f is the mass of the sample at the selected time and S_0 is the initial area of the specimen.

2.2.2. Characterization of the samples

The specimens were characterized after 1000 h of the isothermal test by Scanning Electron Microscopy-Energy Dispersive X-Ray Spectroscopy (SEM-EDX). A JEOL® JSM-820 scanning electron microscope was also used to characterize the morphology and chemical composition of the surface and cross-section of the corroded samples. For cross-sectional SEM analysis, cross-sections of the corroded samples were mounted in a phenolic resin (Buehler®), grinding them with 240, 320, 400, 600, 1000, 2400, and 4000-grit silicon carbide papers. Distilled water was sprayed on the papers during the grinding process.

2.3. LCA methodology

The environmental analysis of study cases was performed by means of the LCA methodology. This methodology is defined according to the ISO 14040 and ISO 14044 standards (ISO 14040, 2006; ISO 14044, 2006) and consists of four sequential stages: (i) goal and scope definition, (ii) inventory analysis, (iii) impact assessment and (iv) interpretation of the results.

2.3.1. Goal and scope definition

This study aimed to assess the environmental impacts of potential construction materials that are in contact with molten salts such as materials for thermal storage tanks. Particularly, this work was a comparative study between uncoated AISI 304 and coated P91 steels, the protective coating being ZrO_2–3 mol%Y_2O_3. In this respect, this study aimed to evaluate sustainable strategies for reducing environmental impacts in the CSP industry.

The system boundary employed was the cradle-to-gate approach. The study cases of this work are currently under research and development phase and operating phase of power plants has not been reported yet, but we have considered this study as starting point.

All material quantities used were included: raw materials, the transport and furnace processes, manufacturing and, in the case of P91 steel, the energy needed in the coating process. Upstream production and handling processes were considered by using the inventory database Ecoinvent 3, which is widely supported by the entire scientific community (Frischknecht and Rebitzer, 2005).

The functional unit was the system to be assessed and all inputs and outputs related to it. The functional unit considered in this study was 1 cm^2 in accordance with the gravimetric analysis performed in the corrosion study, which was focused on 1 cm^2.

Thus, two scenarios were considered and fully analysed: uncoated AISI 304 and coated P91 steels. On the one hand, the uncoated AISI 304 scenario was composed of the AISI 304 austenitic stainless steel with the composition reported in Table 2. On the other hand, the coated P91 scenario was composed of the P91 ferritic-martensitic steel (see Table 2), together with the ZrO_2–3%molY_2O_3 layer.

2.3.2. Life cycle inventory (LCI)

This is an inventory of input/output data with regard to the functional unit. It gathers all the data necessary to meet the goals of the defined study.

Due to the inherent complexity of LCA, transparency is an important guiding principle in executing LCAs to ensure a proper interpretation of the results (Sarkar et al., 2015). In this regard, the functional unit and system boundary must be well established and the inventory publicly available.

Both P91 and AISI 304 steels were modelled based on the Ecoinvent 3 steel, chromium steel 18/8 process. Furnace process, emissions and transports were assumed in the above-mentioned Ecoinvent 3 item. Regarding raw materials, an adaptation was performed by modifying the base alloys towards the required compositions in %wt. (listed in Table 2). Raw materials included not only the alloys involved in each steel but also the iron casting process. Thus, following other steels modelled in Ecoinvent, the iron casting was obtained as a balance between pig iron and iron scrap. The modelled P91 and AISI 304 steel processes were composed of 50 wt.% iron scrap. The balance between iron scrap, alloy elements, and pig iron, resulted in 21.12 wt.% pig iron for AISI 304 steel, and 39.29 wt.% pig iron in P91 steel.

The proposed ZrO_2–3%molY_2O_3 coating was modelled considering the components separately. ZrO_2 was taken from the Ecoinvent 3 database, while Y_2O_3 was modelled based on literature (Huang et al., 2011; Pižl et al., 2017), including the energy wasted in its synthesizing upstream.

The specimens used in the experimental procedure were approximately 5 cm^2. An allocation between specimen's surface and mass was performed to get the needed inputs for the functional unit (1 cm^2). This allocation led to the conclusion that 1 cm^2 is equivalent to 588.654 mg of AISI 304 stainless steel in this scenario and 781.602 mg of P91 steel in the second scenario. In addition, input for the functional unit related to the ZrO_2–Y_2O_3 coating is 0.094 mg cm^{-2}. Table 3 gathers these assumptions, these constituting the LCI of this work.

2.3.3. Impact assessment

The Life Cycle Impact Assessment (LCIA) step estimates the significance of potential environmental impacts of the LCI. The gathered and added inputs/outputs of the system are translated into impact categories. The impact assessment may include the iterative process of reviewing the goal and scope to determine if the objectives of the study have been met (Dissanayake et al., 2009).

In this stage, ISO 14044 explicitly defines mandatory and optional elements. Selection of impact categories, category indicators and characterization models are given as mandatory. Subsequently, classification, which is the assignment of LCI results, and characterization, which is the calculation of the category indicator results, are considered. As optional elements, the standards define Normalization and Weighting. Although many authors discourage it (Schmidt and Sullivan,

Table 3
Amount of material involved in the functional unit. Life cycle assessment inventory.

System	Components in the system	Mass, mg
1 cm^2 of COATED P91	P91	781.602
	Coating	0.094
1 cm^2 of UNCOATED 304	AISI 304	588.654

2002; Pizzol et al., 2017); ISO 14044 (ISO 14044, 2006) indicates that Weighting shall not be used in scientific LCA studies. Since normalization and weighting did not provide relevant information for the goal of the study, they were not conducted.

The selection of impact categories is widely based on the International Reference Life Cycle Data, ILCD recommendations (European Commission, 2012). In this regard, Global Warming Potential and Water Resource Depletion were selected as impact categories in this work. Furthermore, this paper enriched and supplemented the assessment by including the Cumulative Energy Demand (CED) to obtain the total energy consumption throughout the whole process. Despite the environmental benefits of generating electricity from CSP technology, materials involved in these plants consume non-renewable energy and that is why CED category was included. The considered impact categories are described as follows:

- Global Warming Potential represents the Climate Change in kg CO_{2eq} calculating the radiative forcing over a time horizon of 100 years. The Intergovernmental Panel on Climate Change (IPCC) (Change, 2007) implements this method. The Global Warming Potential (GWP) is named Climate Change in the LCA software.
- Water Resource Depletion represents the freshwater scarcity meaning the scarcity-adjusted amount of water used. This category is based on the ecological scarcity method (Frischknecht et al., 2009).
- Cumulative Energy Demand (CED) method has been developed especially for quantifying the energy for a whole process. It is based on the method published by Ecoinvent and expanded for raw materials available in the SimaPro database (Frischknecht and Jungbluth, 2003).

Climate change and increased energy demands are expected to cause frequent and severe strains on the planet (Berardy and Chester, 2017). Furthermore, we are immersed in a severe global water crisis (Hanjra and Qureshi, 2010). Therefore, the selected impact categories play a very significant role in the achievement of sustainable development goals.

The software used was SimaPro (Goedkoop et al., 2016) in its 8th version, together with the inventory database Ecoinvent 3 (Frischknecht and Rebitzer, 2005).

2.3.4. Interpretation

Life cycle interpretation is the final stage of the LCA procedure, in which the results of an LCI or an LCIA, or both, are summarized and discussed as a basis for obtaining conclusions.

3. Results and discussion

3.1. Coating morphology and compositional analysis

The 3 mol% yttria–doped zirconia sol-gel was applied to P91 steel using dip-coating technique and was subsequently subjected to a sintering heat treatment. The resulting coating, together with an uncoated sample, is shown in Fig. 2. As shown in Fig. 2c, the morphology of ZrO_2–Y_2O_3 coating indicates the presence of a jagged and rough surface, which is in agreement with Yang-Il et al. (2015). It consists of a layer that grows by forming agglomerations like a coral, which are embedded within trenches, with a non-uniform thickness that varies between 0.480 μm and 1.100 μm (see Fig. 3). This non-uniformity in thickness may be attributed to the surface preparation (Encinas-Sánchez et al., 2016; Encinas-Sánchez et al., 2015). Furthermore, a diffusion zone was observed, this being a consequence of the thermal treatment to which coatings are subjected during their application. The compositional analysis of the coatings was carried out by energy-dispersive X-ray spectrometry (EDX). Fig. 3 and Table 4 show the atomic percentage of the components determined in the cross-section. This

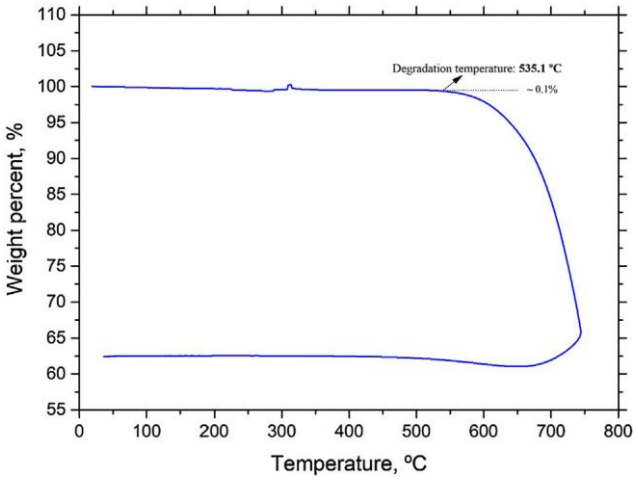

Fig. 1. TGA curve of the prepared salt mixture.

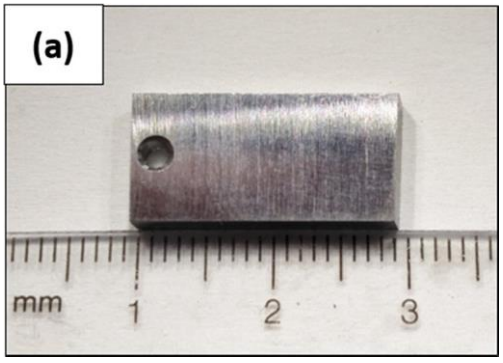

Fig. 2. Surface appearance of coated and uncoated P91 samples before corrosion tests: (a) macrograph of uncoated P91; (b) macrograph of coated P91; (c) SEM micrograph of coated P91.

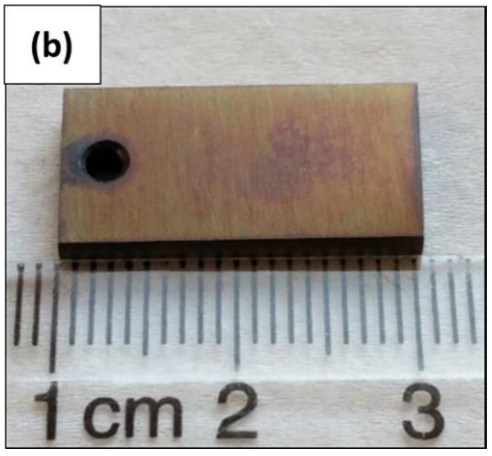

Fig. 2. (*continued*)

analysis clearly indicates the composition of the coating (spectrum 4) and the diffusion zone of the coating (spectra 1 and 2), together with the substrate (spectrum 3).

3.2. Corrosion tests

As previously described, 500 °C was selected as corrosion test temperature. This temperature was selected on the basis of the thermal stability of the salt measured by TGA. Fig. 1 shows the results of the thermogravimetric study. According to this analysis, the salt mixture

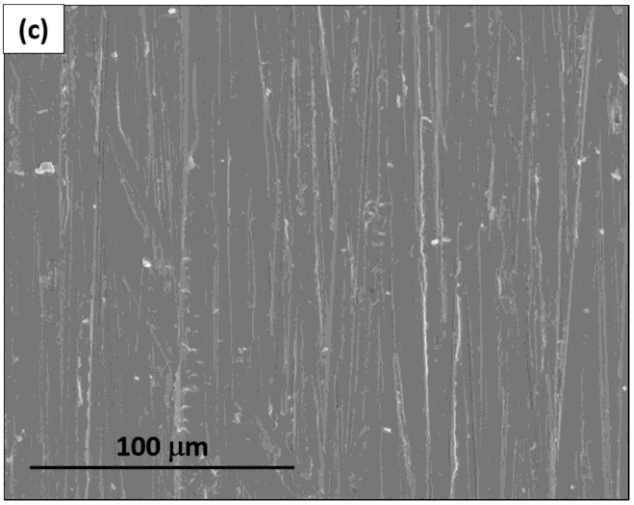

Fig. 2. (*continued*)

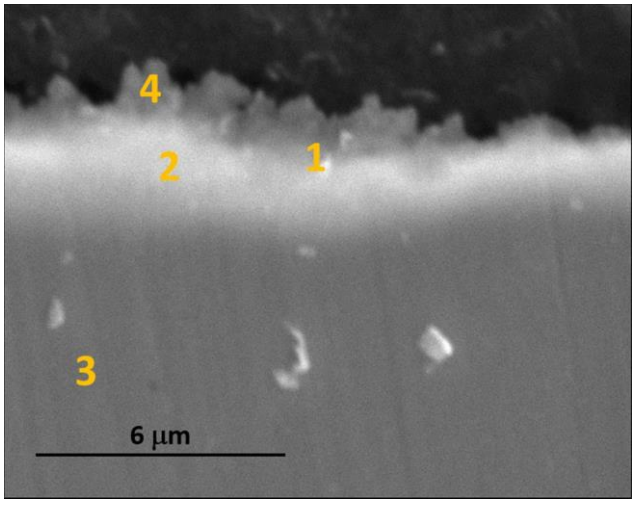

Fig. 3. Cross-section SEM-EDX of coated P91 before corrosion tests.

Table 4
Atomic composition of the coated P91 samples before testing.

Spectrum label	%O	%Cr	%Fe	%Y	%Zr
1	11.71	10.21	75.19	0.21	1.68
2	7.89	8.54	80.95	0.33	2.30
3	–	8.92	91.08		–
4	17.04	9.11	67.80	0.97	5.08

started to degrade at ~ 535 °C (weight loss percentage around 0.1%), which is in agreement with Fernández et al. (Fernández et al., 2012). The commonly considered as maximum operating temperature of Solar Salt® is 565 °C (Kearney and Mahoney, 2002). However, at this temperature the weight loss percentage is higher (around 3%) (Fernández et al., 2012), which explain the differences with the temperature fixed in this work. Furthermore, the maximum operating temperature of Solar Salt® is influenced by several parameters (such as impurity level (Bonk et al., 2018), which may lead to slight differences. Therefore, 500 °C was considered a temperature at which the salt was completely stable, thus avoiding salt additions during test that could affect the stability of the system.

3.2.1. Gravimetric analysis

As described under Section 2.2.1, the samples were analysed via gravimetric analysis during the corrosion test. Their weight was measured after each accumulative immersion interval of 0, 24, 72, 168, 250, 500, 750 and 1000 h.

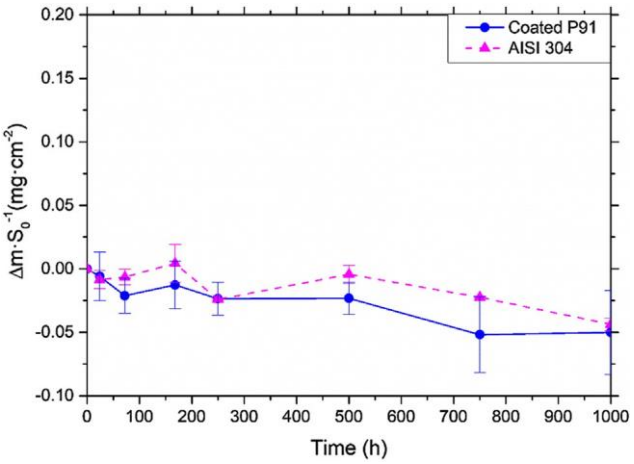

Fig. 4. Gravimetric analysis of the samples in contact with molten Solar Salt at 500 °C.

Fig. 4 shows the gravimetric curve obtained for each sample (uncoated AISI 304 and coated P91). On the one hand, according to other authors (Dorcheh et al., 2016; Dorcheh and Galetz, 2016), P91 steel usually shows a high weight gain, mainly forming iron oxides and iron chromium oxides as corrosion products (Dorcheh et al., 2016; Dorcheh and Galetz, 2016). This statement was substantiated by the gravimetric analysis performed on uncoated P91 samples and gathered in Fig. 5. Thus, it becomes clear that the coating offers a great improvement to this steel, in terms of protection against corrosion in the molten binary salt because after 1000 h of testing coated P91 suffered a weight loss of 0.05007 mg cm^{-2}. This weight loss was mainly due to the excess of coating deposited during the coating process, which is detached during the first hours of testing. Therefore, taking into account this initial behaviour, the weight per unit area only suffered slight losses throughout the test. On the other hand, and according to the gravimetric curve, the behaviour of the coated P91 could be directly comparable to that of the uncoated AISI 304, the weight losses being quite similar (0.05007 and 0.04373 mg cm^{-2} after 1000 h, respectively) despite the fact that the initial weight loss associated with the coatings should not be taken into account. This comparable behaviour would lead to a great economic impact on CSP plants in terms of material costs. However, SEM should corroborate this behaviour.

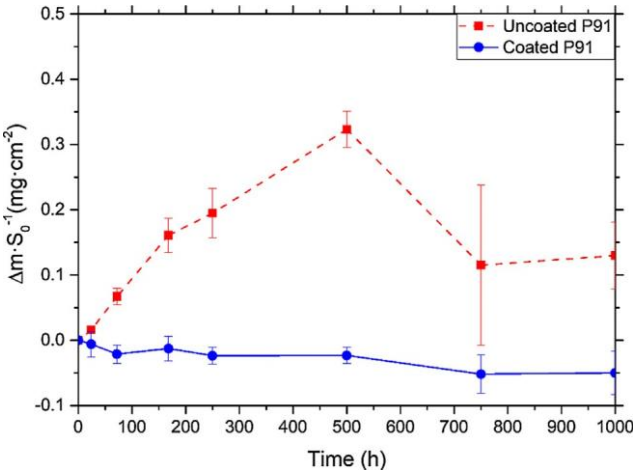

Fig. 5. Comparison of the gravimetric results for coated and uncoated P91 samples in contact with molten Solar Salt at 500 °C.

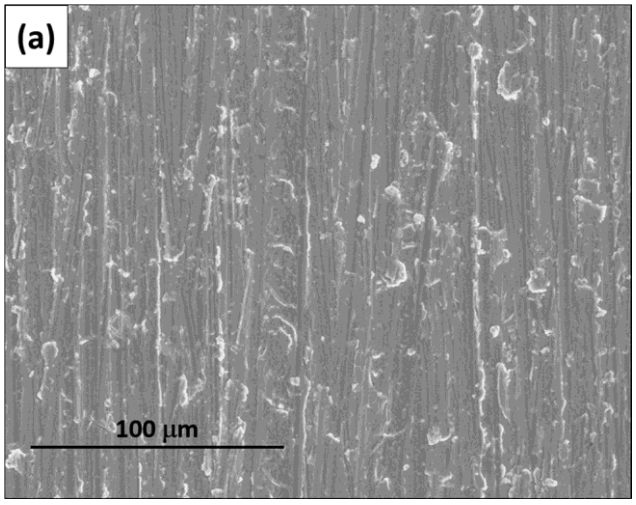

Fig. 6. Superficial SEM micrographs of coated P91 after 1000 h in contact with molten Solar Salt at 500 °C using: (a) secondary electrons; and (b) retrodispersed electrons.

3.2.2. Characterization of the samples

With regard to the coated P91, Fig. 6 shows the surface appearance obtained by SEM. The micrographs were obtained using secondary electrons (see Fig. 6a) and backscattered electrons (see Fig. 6b). Thus, according to the micrographs, the surface appearance after 1000 h of testing showed good compositional homogeneity, although the morphology was not uniform. The latter observation was expected, taking into account the surface appearance before testing (see Fig. 2c). The good surface homogeneity would indicate the good behaviour of the coating after 1000 h of testing, although it was of great interest to analyse the cross-section of the sample in order to determine the composition and morphology of the layer. Thus, Figs. 7 and 8, together with Table 5, showed respectively the cross-section micrograph of a coated sample after testing and the compositional analysis of the cross-section. The micrograph showed a compact layer of coating of thickness ranging between 1.0 and 1.4 μm, the coating layer maintaining 1.68% of Zr and 1.01% of Y (see spectrum 5 in Fig. 7 and Table 5). The coating thickness observed was consistent with the coating thickness and diffusion layer observed on the coated samples before testing. The compaction of the coating layer during the corrosion test is related to the working temperature and diffusion species, which may lead to the formation of compact Fe-Zr compounds (Baron et al., 2008). Furthermore, this compaction could be also due to the initial weight loss

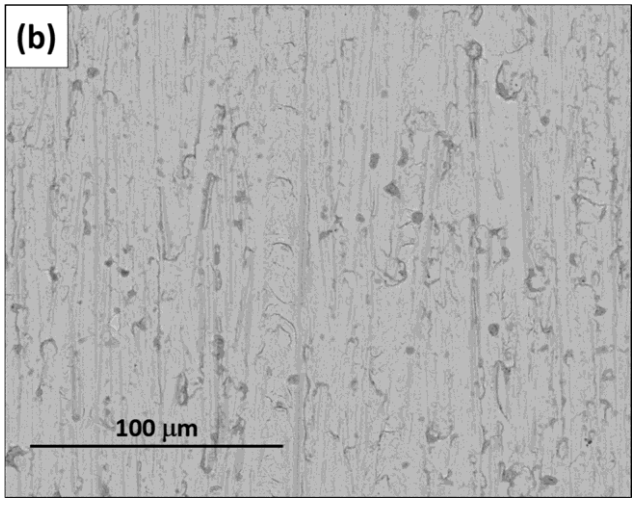

Fig. 6. (*continued*)

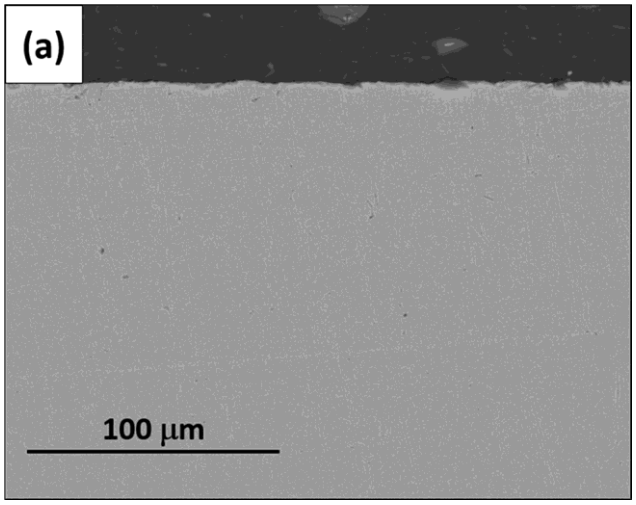

Fig. 7. Cross-section SEM micrographs of coated P91 after 1000 h in contact with molten Solar Salt at 500 °C: (a) secondary electrons; and (b) retrodispersed electrons.

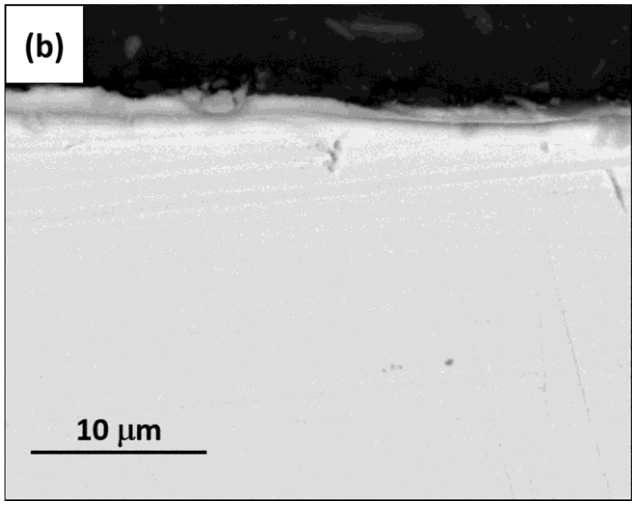

Fig. 7. (*continued*)

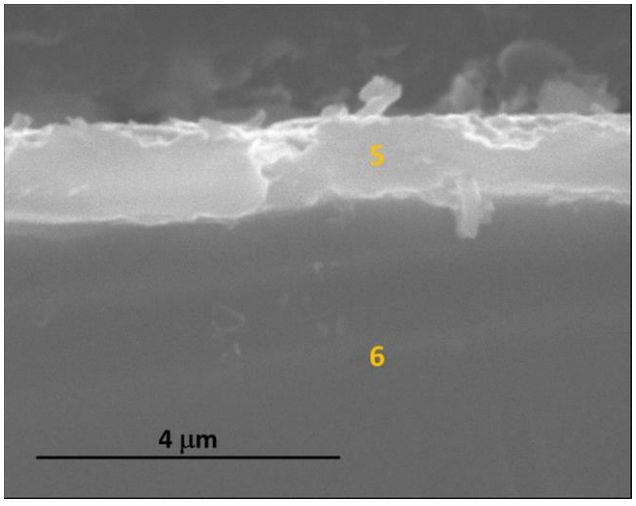

Fig. 8. Cross-section SEM-EDX of coated P91 after 1000 h in contact with molten Solar Salt at 500 °C.

Table 5
Atomic composition of the coated P91 samples after 1000 h of testing.

Spectrum label	%O	%Mg	%Ca	%Cr	%Fe	%Y	%Zr
5	18.32	0.68	0.75	6.90	70.66	1.01	1.68
6	–	–	–	8.32	91.43	–	–

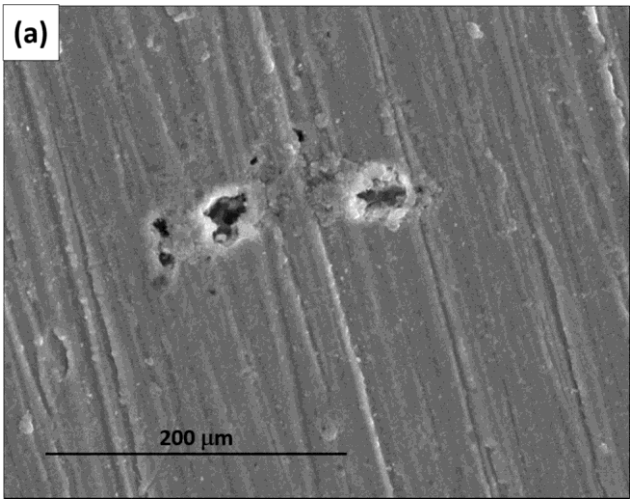

Fig. 9. SEM micrographs of AISI 304 steel after 1000 h in contact with molten Solar Salt at 500 °C: (a) surface appearance; (b) appearance in cross-section.

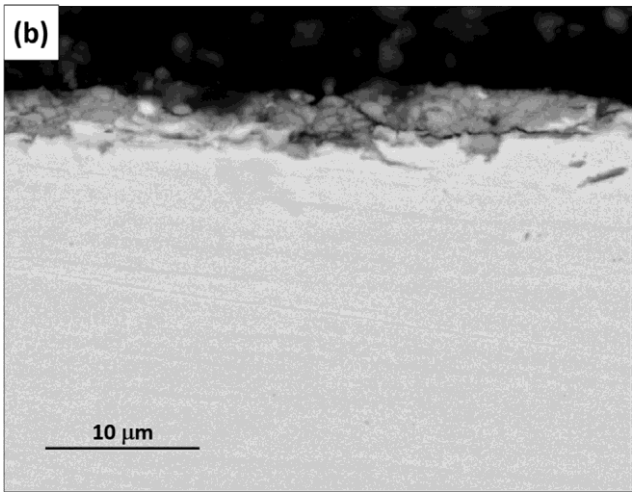

Fig. 9. (*continued*)

observed that lead to a better sintering of the coating layer during test.

Moreover, in order to investigate how the binary molten salt attacked the AISI 304 samples, Fig. 9 shows the surface and the cross-section micrographs. Fig. 9b clearly shows the corrosion layer formed on the surface, its thickness being around 4 μm. This corrosion layer seems to be in contradiction with gravimetric analysis. However, the low weight loss observed in Fig. 4 (lower than 0.05 mg cm^{-2}) could be related to the formation of soluble corrosion products within the molten salt. These corrosion products are typically considered to be in the form of metal chromates (Kerridge and Tariq, 1969). Kruizenga and Gill (2014) confirmed this solubility in nitrate salts and found chromium in the salt. According to Fig. 10 and the compositional values gathered in Table 6, the corrosion layer is constituted by a thin inner layer of a Fe- Cr-O spinel, while the outer layer seems to be formed by iron oxides and Mg-Fe-O compounds. Under this layer, no diffusion of O is observed, with the main content being chromium and iron. These results are consistent with the results obtained by Fernández et al. (2012). These authors concluded that Fe_2O_3 formed in the outer layer together with $MgFe_2O_4$, while $FeCr_2O_4$, which exerts a protective effect on the steel, composed the layer closest to the base material. However, the layer of $MgFe_2O_4$ seemed to be thinner in the present study, which is probably due to a lower impurity level in the Mg. Furthermore, as also determined by Fernández et al. (2012), sodium, potassium and calcium contents were observed in the outer part of the layer, probably due to the formation of insoluble products that are deposited on the sample surfaces (see Fig. 10). This salt accumulation on the top of the samples also reveals a more irregular surface because of the corrosion layer.

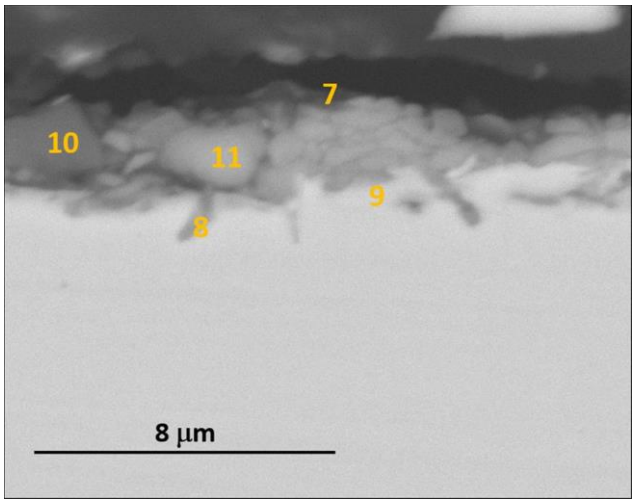

Fig. 10. Cross-section SEM-EDX of AISI 304 steel after 1000 h in contact with molten Solar Salt at 500 °C.

Table 6
Atomic composition of the corrosion layer formed on AISI 304 samples after 1000 h of testing.

Spectrum label	%O	%Na	%Mg	%K	%Ca	%Cr	%Fe	%Ni
7	40.19	0.99	2.45	0.69	0.93	9.06	38.88	6.82
8	2.91	0.32	–	–	0.46	19.99	68.78	7.54
9	2.68	0.67	0.47	–	0.52	18.78	68.53	8.36
10	36.78	0.11	2.11	0.70	2.09	4.83	51.50	1.87
11	21.62	0.57	1.13	0.64	0.89	12.37	59.29	3.49

Thus, the SEM results seem to indicate a good behaviour of the coated P91, results being comparable to those obtained with AISI 304 steel. However, a deeper analysis of the coating layer and substrate should be carried out in order to confirm this statement.

3.3. Environmental analysis

As described under Section 2.3.3, and in order to do an enhanced cradle to grave LCA of 1 cm^2 materials for use at high temperature in CSP application, three different impacts were evaluated in two possible scenarios. These scenarios were called: Uncoated 304, and Coated P91.

The characterization results taking into account the three impact categories assessed are summarized in Table 7 and Fig. 11.

In all the assessed impact categories, Coated P91 obtained better results in comparison with Uncoated 304. Moreover, by considering the

Table 7
LCA characterization results.

Impact category	Unit	UNCOATED 304	COATED P91
Cumulative energy demand	MJ	$5.494 \cdot 10^{-2}$	$3.800 \cdot 10^{-2}$
Climate change	kg CO_2 eq	$3.894 \cdot 10^{-3}$	$2.854 \cdot 10^{-3}$
Water resource depletion	m^3 H_2O eq	$2.773 \cdot 10^{-2}$	$1.707 \cdot 10^{-2}$

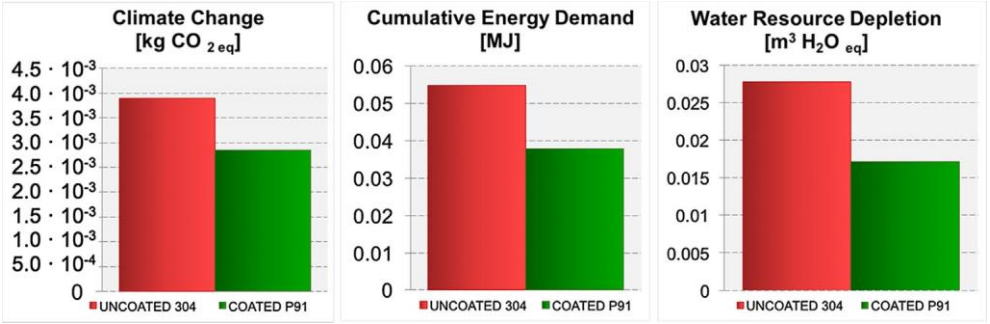

Fig. 11. LCA characterization results.

functional unit choice, steel mg content was higher in the case of Coated P91 than in Uncoated 304 (see Table 3). Nonetheless, the impacts remain lower for Coated P91. In the Functional Unit, the lower amount of AISI 304 steel showed higher impacts than the larger amount of P91 steel, which highlights the environmental benefits of using P91 (isolated and coated) in place of AISI 304.

The Global Warming Potential of the Uncoated 304 system was calculated as $3.894 \cdot 10^{-3}$ kg $CO_{2\ eq}$. On the other hand, the Global Warming Potential of the Coated P91 system was $2.854 \cdot 10^{-3}$ kg $CO_{2\ eq}$. Thus, the choice of Coated P91 system would have a significantly lower impact and it would effectively address the Climate Change problems.

Regarding Cumulative Energy Demand, an impact of $5.494 \cdot 10^{-2}$ MJ was measured in the case of Uncoated 304. Results revealed that the use of Coated P91 led to a reduction of the total energy consumption by 30.84%.

In the case of Water Scarcity Indicator, the comparative LCA results showed that about 38.44% less water resource was required, with a saving of $1.066 \cdot 10^{-2}$ m^3 $cm_{H2O\ eq}^2$, using Coated P91 instead of Uncoated 304.

Taking into account the previous results, a thorough analysis of the main contributions to the whole environmental impact assessment was accomplished. To this end, a detailed environmental analysis of Uncoated 304 is described in Fig. 12. Likewise, Fig. 13 details the main environmental impact contributors of Coated P91.

A detailed environmental analysis was performed on Coated P91 in a similar way to Uncoated 304. In addition to the parameters analysed in the case of Uncoated 304, the study of Coated P91 included both the substrate and the coating in the evaluation. Fig. 13 shows the impacts associated with each component considered in the LCA. The highest impact was again due to the Cr, especially in Water Resource Depletion indicator, where Cr was the cause of 88.16% of the water depletion. The relative contribution of Molybdenum in the environmental profile depended on its weight composition. It is possible to notice how the small wt.% contribution (0.85 wt.%) could give rise impacts close to 10% in Global Warming Potential and Water Resource Depletion and 7.66% in the Cumulative Energy Demand indicator. Thus, the coating became of particular interest. According to all the results, the protective layer clearly improved the corrosion resistance and its environmental evaluation achieved very good results. Among the impact categories assessed, none of them obtained more than 0.03%. That means that less than 0.03% of the complete impacts were due to the coating.

Finally, elements with higher wt.% content in the steel composition, such as pig iron, did not have a great influence on the environmental impacts. The impacts were 0.16–7.04% in the case of Uncoated 304 and 0.63–23.71% in the case of Coated P91. These inputs, which are not described in Figs. 12 and 13, do not contribute to the environmental burdens or are collected in the "Rest" item.

The assessment showed that the Uncoated 304 system had a higher environmental impact in comparison to Coated P91. Those components that contributed to the highest burden in the 304 system were Cr and Ni. Table 2 lists the chemical composition (in wt.%) of AISI 304 and P91 steels, where it can be seen that the Cr-Ni contents of ~18–8 are lower in the AISI 304 than the ~8–0 in the P91. In other words, the reduction in the weight percentage of higher impact contributors can greatly affect the overall environmental impact of the whole system. Thus, the lower the Cr-Ni content, the lower the environmental impacts.

4. Conclusions

This research not only assessed and quantified corrosion resistance of the uncoated 304 steel and the effect of the ZrO_2–3%molY_2O_3 coating on P91 steel but also assessed, quantified and compared the environmental impacts of both systems. The linked technical-environmental quantification provided in the present paper highlights the importance of considering the whole assessment when conducting a material selection process for CSP applications.

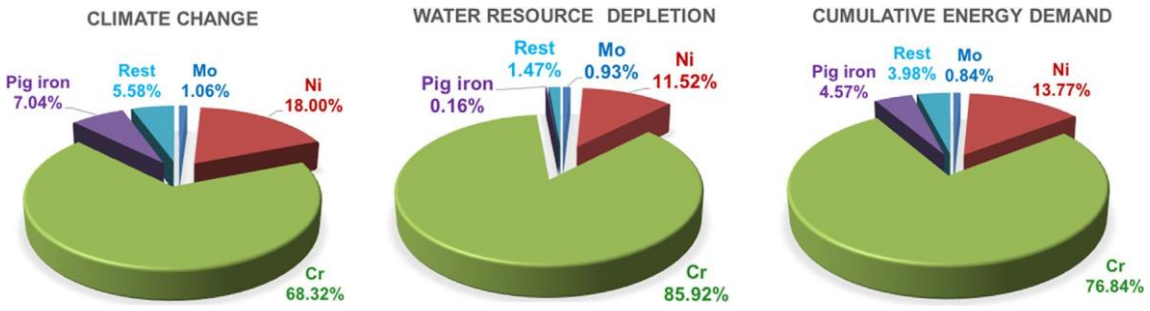

Fig. 12. Detailed environmental contribution (%) of the components in the case of Uncoated 304.

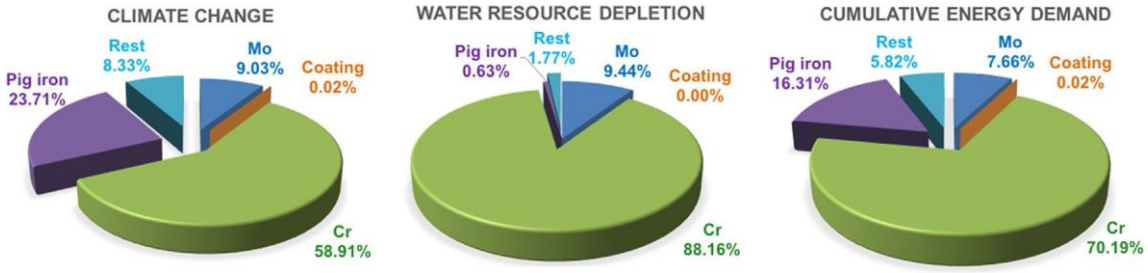

Fig. 13. Detailed environmental contribution (%) of the components in the case of Coated P91.

In terms of corrosion evaluation, from a gravimetric point of view, the behaviour of the coated P91 was directly comparable to that of the uncoated 304, the weight losses being quite similar (0.05007 and 0.04373 mg cm^{-2}, respectively). SEM micrographs revealed the maintenance of a compact coating layer, with a thickness ranging between 1.0 and 1.4 μm. These results clearly show the good behaviour of the coated samples. In fact, corrosion behaviour for the coated P91 seems to be comparable to uncoated 304 steel, although deeper studies should be performed. Thus, from the technical point of view, the use of the coated P91 scenario could be workable in CSP high-temperature applications.

In terms of environmental analysis, an extensive LCA was performed and the results showed the better environmental suitability of Coated P91 against Uncoated AISI 304. Thus, the use of Coated P91 system resulted in a reduction in the environmental burden and numerous advantages. Specifically, Coated P91 decreased the overall total environmental impact by 26.72% in the Global Warming Potential, 30.84% in the Cumulative Energy Demand and 38.44% in the Water Resource Depletion measures.

Results revealed that environmental benefits could be obtained by using lower Cr-Ni content steel for all the impact categories assessed. Furthermore, the ZrO_2–Y_2O_3 coating not only improved corrosion resistance but also had a negligible environmental impact (its influence was below 0.03%), which demonstrates its technical and environmental appropriateness.

References

Amri, Amun, Jiang, Zhong-Tao, Pryor, Trevor, Yin, Chun-Yang, Xie, Zonghan, Mondinos, Nick, 2012. Surf. Coat. Technol. 207, 367–374.

Baron, Y.S., Ruiz, A., Navas, G., 2008. High temperature oxidation resistance of 1.25Cr-0.5Mo wt.% steels by zirconia coating. Surf. Coat. Technol. 202, 2616–2622.

Batuecas, E., Mayo, C., Díaz, R., Pérez, F.J., 2017. Life cycle assessment of heat transfer fluids in parabolic trough concentrating solar power technology. Sol. Energy Mater. Sol. Cells 171, 91–97.

Berardy, A., Chester, M.V., 2017. Climate change vulnerability in the food, energy, and water nexus: concerns for agricultural production in Arizona and its urban export supply. Environ. Res. Lett. 12, 035004.

Bonk, A., Sau, S., Uranga, N., Hernaiz, M., Bauer, T., 2018. Advanced heat transfer fluids for direct molten salt line-focusing CSP plants. Prog. Energy Combust. Sci. 67, 69–87.

Bradshaw, R. W., Goods, S.H., 2001. Corrosion resistance of stainless steels during thermal cycling in alkali nitrate molten salts. Sandia Report. SAND2001-8518.

Change, 2007. IPCC Climate. The Fourth Assessment Report of the Intergovernmental Panel on Climate Change, Geneva, Switzerland.

Choudhury, P., Agrawal, D.C., 2011. Sol–gel derived hydroxyapatite coatings on titanium substrates. Surf. Coat. Technol. 206, 360–365.

Croll, S.G., 1979. J. Appl. Polym. Sci. 23, 847.

de Miguel, M.T., Encinas-Sánchez, V., Lasanta, M.I., García-Martín, G., Pérez, F.J., 2016. Corrosion resistance of HR3C to a carbonate molten salt for energy storage applications in CSP plants. Sol. Energy Mater. Sol. Cells 157, 966–972.

Díaz-Parralejo, A., Ortiz, A.L., Caruso, R., 2010. Effect of sintering temperature on the microstructure and mechanical properties of ZrO_2-3 mol%Y_2O_3 sol–gel films. Ceram. Int. 36, 2281–2286.

Dissanayake, N., Summerscales, J., Grove, S., Singh, M., 2009. Life cycle assessment of flax fibers for the reinforcement of composites. J. Biobased Mater. Bioenergy 3, 245–248.

Dorcheh, A.S., Durham, R.N., Galetz, M.C., 2016. Corrosion behaviour of stainless and low-chromium steels and IN625 in molten nitrate salts at 600 °C. Sol. Energy Mater. Sol. Cells 144, 109–116.

Dorcheh, A.S., Galetz, M.C., 2016. Slurry aluminizing: a solution for molten nitrate salt corrosion in concentrated solar power plants. Sol. Energy Mater. Sol. Cells 146, 8–15.

Eloneva, S., Puheloinen, E.M., Kanerva, J., Ekroos, A., Zevenhoven, R., Fogelholm, C.J., 2010. Co-utilisation of CO_2 and steelmaking slags for production of pure $CaCO_3$-legislative issues. J. Cleaner Prod. 18, 1833–1839.

Encinas-Sánchez, V., Macías-García, A., Díaz-Díez, M.A., Brito, P., Cardoso, D., 2015. Influence of the quality and uniformity of ceramic coatings on corrosion resistance. Ceram. Int. 41, 5138–5146.

Encinas-Sánchez, V., Macías-García, A., Díaz-Díez, M.A., Díaz-Parralejo, A., 2016. Characterization of sol-gel coatings deposited on a mechanically treated stainless steel by using a simple non-destructive electrical method. J. Ceram. Soc. Jpn. 124, 185–191.

Encinas-Sánchez, V., Macías-García, A., Pérez, F.J., 2017. Effect of withdrawal rate on the evolution of optical properties of dip-coated yttria-doped zirconia thin films. Ceram. Int. 43, 13094–13100.

Encinas-Sánchez, V., de Miguel, M.T., García-Martín, G., Lasanta, M.I., Pérez, F.J., 2018. Corrosion resistance of Cr/Ni alloy to a molten carbonate salt at various temperatures for the next generation high-temperature CSP plants. Sol. Energy 171, 286–292.

European Commission – Joint Research Centre – Institute for Environment and Sustainability, 2012. International reference life cycle data system (ILCD) handbook – recommendations for life cycle impact assessment in the European context. Publications Office of the European Union, Luxemburg.

Fernández, A.G., Lasanta, M.I., Pérez, F.J., 2012. Molten salt corrosion of stainless steels and low-Cr steel in CSP plants. Oxid. Met. 78, 329–348.

Frischknecht, R., Jungbluth, N., et al., 2003. Implementation of Life Cycle Impact Assessment Methods. Final Report Ecoinvent 2000, Swiss Centre for LCI. Duebendorf, CH < http://www.ecoinvent.ch >.

Frischknecht, R., Steiner, R., Jungbluth, N., 2009. The Ecological Scarcity Method–Eco-Factors 2006 – A Method for Impact assessment in LCA, 1–188.

Frischknecht, R., Rebitzer, G., 2005. The ecoinvent database system: a comprehensive web-based LCA database. J. Cleaner Prod. 13, 1337–1343.

Fuqiang, W., Ziming, C., Jianyu, T., Yuan, Y., Yong, S., Linhua, L., 2017. Progress in concentrated solar power technology with parabolic trough collector system: a comprehensive review. Renew. Sustain. Energy Rev. 79, 1314–1328.

García-Martín, G., Lasanta, M.I., Encinas-Sánchez, V., de Miguel, M.T., Pérez, F.J., 2017. Evaluation of corrosion resistance of A516 Steel in a molten nitrate salt mixture using a pilot plant facility for application in CSP plants. Sol. Energy Mater. Sol. Cells 161, 226–231.

Giglioa, A., Lanzinia, A., Leonea, P., Rodríguez García, M.M., Zarza Moya, E., 2017. Direct steam generation in parabolic-trough collectors: a review about the technology and a thermo-economic analysis of a hybrid system. Renew. Sustain. Energy Rev. 74, 453–473.

Goedkoop, M., Oele, M., Leitjting, J, Ponsioen, T., Meijer, E., 2016. Introduction to LCA with SimaPro, Report version 5.2.

González-Roubaud, E., Pérez-Osorio, D., Prieto, C., 2017. Review of commercial thermal energy storage in concentrated solar power plants: steam vs. molten salts. Renew. Sustain. Energy Rev. 80, 133–148.

Goods, S.H., Bradshaw, R.W., 2004. Corrosion of stainless steels and carbon steel by molten mixtures of commercial nitrate salts. J. Mater. Eng. Perform. 3, 78–87.

Grosu, Y., Udayashankar, N., Bondarchuk, O., González-Fernández, L., Faik, A., 2018. Unexpected effect of nanoparticles doping on the corrosivity of molten nitrate salt for thermal energy storage. Solar Energy Mater Solar Cells 178, 91–97.

Grosu, Y., Bondarchuk, O., Faik, A., 2018. The effect of humidity, impurities and initial state on the corrosion of carbon and stainless steels in molten HitecXL salt for CSP application. Sol. Energy Mater. Sol. Cells 174, 34–41.

Hamden, Z., Boufi, S., Conceiçao, D.S., Ferraria, A.M., Botelho do Rego, A.M., Ferreira, D.P., Vieira-Ferreira, L.F., Bouattour, S., 2014. Li-N doped and codoped TiO_2 thin films deposited by dip-coating: characterization and photocatalytic activity under halogen lamp. Appl. Surf. Sci. 314, 910–918.

Hanjra, M.A., Qureshi, M.E., 2010. Global water crisis and future food security in an era of climate change. Food Policy 35, 365–377.

He, Kun, Wang, Li, 2017. A review of energy use and energy-efficient technologies for the iron and steel industry. Renew. Sustain. Energy Rev. 70, 1022–1039.

Huang, M., Kai, G., Zhenyong, M., Haohong, C., Xinxin, Y., Fangfang, X., Jingtai, Z., 2011. Morphology controllable synthesis of yttrium oxide-based phosphors from yttrium citrate precursors. J. Rare Earths 29, 830–836.

ISO 14040, 2006. Environmental Management – Life Cycle Assessment – Principles and Framework. Geneva, Switzerland.

ISO 14044, 2006. Environmental Management – Life Cycle Assessment – Requirements and Guidelines. Geneva, Switzerland.

Jin, J., Ling, Y., Hao, Y., 2017. Similarity analysis of parabolic-trough solar collectors. Appl. Energy 204, 958–965.

John-Berlin, I., Sujatha-Lekshmy, S., Ganesan, V., Thomas, P.V., Joy, K., 2014. Effect of

Mn doping on the structural and optical properties of ZrO_2 thin films prepared by sol-gel method. Thin Solid Films 550, 199–205.

Johnson, B.Y., Edington, J., Williams, A., O'Keefe, M.J., 2005. Mater. Charact. 54, 41–48.

Kamalan-Kirubaharan, A.M., Kuppusami, P., Priya, R., Divakar, R., Gupta, M., Pandit, D., Ningshen, S., 2018. Synthesis, microstructure and corrosion behavior of compositionally graded Ni-YSZ diffusion barrier coatings on inconel-690 for applications in high temperature environments. Corros. Sci. 135, 243–254.

Kearney, D., Mahoney, R., 2002. Assessment of a molten heat transfer fluid in a parabolic trough solar field. Solar Energy Eng. 125, 170–176.

Kerridge, D.H., Tariq, S.A., 1969. Molten sodium nitrite-potassium nitrite eutectic: the reactions of some compounds of chromium. Inorganica Chimica Acta 3, 667–670.

Kruizenga, A., Gill, D., 2014. Corrosion of iron stainless steels in molten nitrate salt. Energy Procedia 49, 878–887.

Liu, M., Steven Tay, N.H., Bell, S., Belusko, M., Jacob, R., Will, G., Saman, W., Bruno, F., 2016. Review on concentrating solar power plants and new developments in high temperature thermal energy storage technologies. Renew. Sustain. Energy Rev. 53, 1411–1432.

Mimura, K., Kato, K., 2013. Jpn. J. Appl. Phys. 52.

Pacheco, J.E., Bradshaw, R.W., Dawson, D.B., de la Rosa, W., Gilbert, R., Goods, S.H., Hale, M.J., Jacobs, P., Jones, S.A., Kolb, G.J., Prairie, M.R., Reilly, H.E., Showalter, S. K., Vant-Hull, L.L., 2002. Final Test and Evaluation Results from the Solar Two Project, Sandia National Laboratories, Albuquerque, NM 87185-0703.

Pižl, M., Jankovský, O., Ulbrich, P., Szabó, N., Hoskovcová, I., Sedmidubský, D., Bartůněk, V., 2017. Facile preparation of nanosized yttrium oxide by the thermal decomposition of amorphous Schiff base yttrium complex precursor. J. Organomet. Chem. 830, 146–149.

Pizzol, M., Laurent, A., Sala, S., Weidema, B., Verones, F., Koffler, C., 2017. Normalisation and weighting in life cycle assessment: quo vadis? Int. J. Life Cycle Assess. 22, 853–866.

Pizzolato, A., Donato, F., Verda, V., Santarelli, M., 2015. CFD-based reduced model for the simulation of thermocline thermal energy storage systems. Appl. Therm. Eng. 76, 391–399.

Ruiz-Cabañas, F.J., Prieto, C., Madina, V., Fernández, I., Cabeza, L.F., 2017. Materials selection for thermal energy storage systems in parabolic trough collector solar facilities using high chloride content nitrate salts. Sol. Energy Mater. Sol. Cells 163, 134–147.

Sarkar, D., Datta, R., Mukherjee, A., Hannigan, R., 2015. An Integrated Approach to Environmental Management. John Wiley & Sons.

Schmidt, W.P., Sullivan, J., 2002. The value debate: weighting of life cycle assessments in a global context: global diversity exists and has to be valued. Int. J. Life Cycle Assess. 7, 250 250-250.

Vignarooban, K., Xu, X., Arvay, A., Hsu, K., Kannan, A.M., 2015. Heat transfer fluids for concentrating solar power systems: a review. Appl. Energy 146, 383–396.

Wang, D., Bierwagen, G.P., 2009. Sol-gel coatings on metals for corrosion protection. Prog. Org. Coat. 64, 327–338.

Yang-Il, J., Hyun-Gil, K., Jeong-Yong, P., Dong-Jun, P., Jung-Hwan, P., 2015. Effect of heat-treatment on phase formation and crystallization of sol–gel derived Al_2O_3, ZrO_2–Y_2O_3, and Ta_2O_5 oxide coatings. J. Asian Ceram. Soc. 3, 217–220.

Zaversky, F., García-Barberena, J., Sánchez, M., Astrain, D., 2013. Transient molten salt two-tank thermal storage modeling for CSP performance simulations. Sol. Energy 93, 294–311.

Zhao, C.Y., Wu, Z.G., 2011. Thermal property characterization of a low melting-temperature ternary nitrate salt mixture for thermal energy storage systems. Sol. Energy Mater. Sol. Cells 95, 3341–3346.